



**HAL**  
open science

# Asymmetric Franck-Condon factors in suspended carbon nanotube quantum dots

F. Cavaliere, E. Mariani, Renaud Leturcq, C. Stampfer, M. Sassetti

► **To cite this version:**

F. Cavaliere, E. Mariani, Renaud Leturcq, C. Stampfer, M. Sassetti. Asymmetric Franck-Condon factors in suspended carbon nanotube quantum dots. *Physical Review B: Condensed Matter and Materials Physics (1998-2015)*, 2010, 81 (20), pp.201303(R). 10.1103/PhysRevB.81.201303 . hal-00549039

**HAL Id: hal-00549039**

**<https://hal.science/hal-00549039>**

Submitted on 15 Jul 2022

**HAL** is a multi-disciplinary open access archive for the deposit and dissemination of scientific research documents, whether they are published or not. The documents may come from teaching and research institutions in France or abroad, or from public or private research centers.

L'archive ouverte pluridisciplinaire **HAL**, est destinée au dépôt et à la diffusion de documents scientifiques de niveau recherche, publiés ou non, émanant des établissements d'enseignement et de recherche français ou étrangers, des laboratoires publics ou privés.

# Asymmetric Franck-Condon factors in suspended carbon nanotube quantum dots

Fabio Cavaliere<sup>1</sup>, Eros Mariani<sup>2,3</sup>, Renaud Leturcq<sup>4,5</sup>, Christoph Stampfer<sup>4,6</sup> and Maura Sassetti<sup>1</sup>

<sup>1</sup> CNR-SPIN and Dipartimento di Fisica, Università di Genova, Via Dodecaneso 33, 16146 Genova, Italy

<sup>2</sup> Institut für Theoretische Physik, Freie Universität Berlin, Arnimallee 14, 14195 Berlin, Germany

<sup>3</sup> School of Physics, University of Exeter, Stocker Road, Exeter, EX4 4QL, United Kingdom

<sup>4</sup> Laboratory for Solid State Physics, ETH Zurich, 8093 Zurich, Switzerland

<sup>5</sup> IEMN CNRS-UMR 8520, ISEN, Avenue Poincaré, BP 60069, 59652 Villeneuve d'Ascq Cedex, France

<sup>6</sup> JARA-FIT and II. Institute of Physics, RWTH Aachen University, 52074 Aachen, Germany

(Dated: March 20, 2021)

Electronic states and vibrons in carbon nanotube quantum dots have in general different location and size. As a consequence, the conventional Anderson-Holstein model, coupling vibrons to the dot total charge only, may no longer be appropriated in general. Here we explicitly address the role of the spatial fluctuations of the electronic density, yielding *space-dependent* Franck-Condon factors. We discuss the consequent marked effects on transport which are compatible with recent measurements. This picture can be relevant for tunneling experiments in generic nano-electromechanical systems.

PACS numbers: 73.23.-b; 85.85.+j; 78.32.-k

*Introduction* — Advances in miniaturization paved the way to the fabrication of nanodevices in which molecular systems become active elements of circuits [1]. Tunneling of electrons through molecules leads to the excitation/de-excitation of quantized vibrational modes (vibrons) which have been experimentally observed in suspended carbon nanotubes (CNT) [2–5]. Their remarkable electronic and vibronic properties allowed for the observation of breathing [2] and stretching vibrons [3, 4] in recent transport experiments.

In general vibrons couple *both* to the total dot charge *and* to the spatial fluctuations of the electron density. The latter received limited attention so far [6–8]. In most cases the Anderson-Holstein (AH) model [9, 10] has been employed, in which the vibron couples *only* to the total charge. The AH model yields *position-independent* Franck-Condon (FC) factors [11] which strongly affect transport [12–14]. The predicted current suppression at low bias and the intensity of the vibrational sidebands have been confirmed in a recent experiment on suspended CNT quantum dots [4].

In this paper we show that the effects of density fluctuations are crucial when the size and location of the dot and of the vibron do not coincide. They are indeed dramatic when the vibron size  $L_v$  is *smaller* than the dot size  $L_d$ : here, in sharp contrast with the AH model, *position-dependent* FC factors arise, possibly *asymmetric* on the dot tunneling barriers. This has profound consequences on the transport properties of the system. Only when  $L_v > L_d$ , the total charge contribution is dominant and an effective AH model may be justified [15].

Our predictions find an important confirmation in further measurements on the device considered in Ref. 4. A scanning electron microscope image, Fig. 1a, shows the CNT connected to source (S) and drain (D) leads. A central suspended electrode (TG) acts as an electrically insulated top-gate, below which a quantum dot is formed (for more details see Ref. 4). Transport mea-

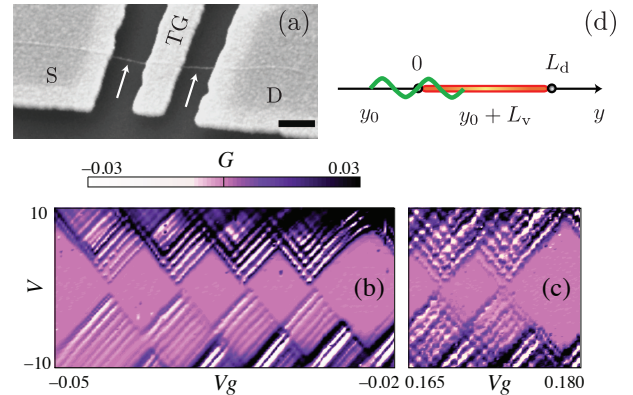


FIG. 1: (Color online) (a) Scanning electron microscope of the suspended CNT (arrows denote its position) connected to source (S) and drain (D) contacts. A top gate (TG) is also present. Scale bar: 200 nm. (b,c) Experimentally determined differential conductance  $G$  (units  $e^2/h$ ) as a function of the top gate voltage  $V_g$  (units V) and bias  $V$  (units mV). (d) Schematic view of the coupled quantum dot-vibron system. The thick part represents the quantum dot and the wiggly line the vibron.

surements have been performed in a pumped  $^4\text{He}$  cryostat with a standard lock-in technique. The differential conductance  $G$  (Figs. 1b,c) exhibits an almost perfect fourfold degeneracy in the Coulomb blockade diamonds and a rich structure of sidebands due to the excitation of stretching vibrons. The energy of electronic excited states measured on the Coulomb diamonds yields a dot size  $L_d \approx 240$  nm, while the separation of vibrational subbands of about 0.8 meV yields  $L_v \approx 60$  nm  $< L_d$  [4]. A striking feature is the *suppression of vibrational sidebands with negative slope* as the gate voltage is varied. While in Fig. 1c, with  $V_g$  in the regime analyzed in Ref. 4, sidebands with both slopes are present, in Fig. 1b for  $V_g < 0$  those with negative slope are completely absent. Here we show that this behaviour requires *asymmetric* FC factors at the tunneling barriers between the dot and

the leads. We stress that such a suppression *cannot* be obtained within the AH model, even assuming strongly asymmetric tunnel barriers. The case of Fig. 1c is on the other hand consistent with quasi-symmetric FC factors, in the spirit of the standard AH model.

In addition, an alternating pattern of positive and negative differential conductance (PDC/NDC) is observed in all the explored voltage ranges. This fact will be explained in terms of a *dynamical trapping* of dot states induced by asymmetries in the tunnel barriers.

*CNT Dot-vibron model* — As a model for our system, we consider a quantum dot confined between  $y_1 = 0$  and  $y_2 = L_d$  along the CNT and a vibron clamped at  $y_0$  and  $y_0 + L_v$ , with  $-L_v < y_0 < L_d$  for a finite overlap between the two systems (see Fig. 1d). We describe the CNT-quantum dot as a Luttinger liquid with two valleys  $\eta = \pm 1$  and two spin channels  $\sigma = \pm 1$  [16] employing standard bosonization techniques with open boundaries [17, 18] (i.e. the electronic field satisfies  $\psi_{\eta,\sigma}(0) = \psi_{\eta,\sigma}(L_d) = 0$ ). The bosonization picture is not essential in our analysis, but it simplifies considerably the formal treatment of the electron-vibron coupling. The dot Hamiltonian is composed of three terms  $H_d = H_d^{(0)} + H_d^{(1)} + H_d^{(2)}$  ( $\hbar = 1$ ,  $\mu \in \{c+, c-, s+, s-\}$ )

$$\begin{aligned} H_d^{(0)} &= \frac{E_c}{8}(N_{c+} - N_g)^2 + \frac{\pi v_F}{8L_d}(N_{c-}^2 + N_{s+}^2 + N_{s-}^2), \\ H_d^{(1)} &= \frac{1}{2} \sum_{\mu} \sum_{q=1}^{\infty} (p_{\mu,q}^2 + \omega_{\mu,q}^2 x_{\mu,q}^2), \\ H_d^{(2)} &= \frac{\Delta\varepsilon}{2}(N_{c+} - N_{c-}). \end{aligned}$$

The term  $H_d^{(0)}$  describes the energy of  $N_{c+}$  electrons in the dot for a given configuration with  $N_{\eta\sigma}$  electrons with spin  $\sigma$  in branch  $\eta$ . Here, total (+) and relative (-) charge ( $c$ ) and spin ( $s$ ) modes have been introduced [16], with  $N_{c+} = \sum_{\eta\sigma} N_{\eta\sigma}$ ,  $N_{c-} = \sum_{\eta\sigma} \eta N_{\eta\sigma}$ ,  $N_{s+} = \sum_{\eta\sigma} \sigma N_{\eta\sigma}$  and  $N_{s-} = \sum_{\eta\sigma} \eta\sigma N_{\eta\sigma}$ . In addition,  $N_g \propto V_g$  is the charge induced by the top-gate voltage  $V_g$ ,  $E_c$  is the charging energy and  $v_F$  the Fermi velocity [19]. Collective charge and spin excitations are described as bosonic modes in  $H_d^{(1)}$ . The generalized position and momentum of mode  $\mu$  are respectively  $x_{\mu,q}$  and  $p_{\mu,q}$ , with frequency  $\omega_{\mu,q} = \pi v_{\mu} q / L_d$  and group velocity  $v_{\mu}$  [19]. Finally,  $H_d^{(2)}$  models a shift between the energy of the two valleys [20]. The lowest stretching vibron is described by the harmonic Hamiltonian  $H_v = p_0^2/2M + M\omega_0^2 x_0^2/2$ , where  $M$  is the vibron mass,  $\omega_0 = \pi v_s / L_v$  its frequency and  $v_s$  the stretching mode velocity [19]. Here,  $x_0$  is the amplitude of the lowest vibron, with distortion field  $u(y) = \sqrt{2}x_0 \sin[\pi(y - y_0)/L_v]$  along the CNT, and  $p_0$  is the conjugate momentum. In a CNT,  $v_s < v_{\mu}$  and the experimental estimates yield  $\omega_0 < \omega_{\mu,1}$  [3, 4].

Electrons and vibrations are microscopically coupled via

$$H_{d-v} = c \int_{\max[0, y_0]}^{\min[L_d, y_0 + L_v]} dy [\rho_R^{(c+)}(y) + \rho_R^{(c+)}(-y)] \partial_y u(y), \quad (1)$$

where  $c$  is the deformation potential coupling constant [19, 21, 22] and we have introduced the total electron density of right movers  $\rho_R^{(c+)}(y) = \sum_{\eta,\sigma} \psi_{R,\eta,\sigma}^\dagger(y) \psi_{R,\eta,\sigma}(y)$  with  $\psi_{R,\eta,\sigma}(y)$  their Fermi operator [23, 24]. Notice that, while vibrations couple to the  $c+$  mode only, all four collective electronic modes are important for transport. In bosonized form, one has  $\rho_R^{(c+)}(y) = (N_{c+}/2L_d) + (1/2\pi) \partial_y \phi_{c+}(y)$  with  $\phi_{c+}(y) = \sqrt{\omega_{c+,1}/2} \sum_{q>0} e^{-\xi\pi q y / 2L_d} [e^{-i\pi q y / L_d} (x_{c+,q} - i\omega_{c+,q}^{-1} p_{c+,q}) + \text{h.c.}]$  and  $\xi$  the short wavelength cutoff. This expression of the density neglects the fast oscillating terms due to mixed right and left-moving fermion fields and is reliable in the large total charge  $N_{c+}$  regime with  $N_{c+} \gg L_d/\pi L_v$ . This condition is experimentally satisfied in all the ranges of parameters analyzed in this paper. The coupling Eq. (1) can thus be decomposed into  $H_{d-v}^{(N)} = c_0 x_0 N_{c+}$  and  $H_{d-v}^{(pl)} = x_0 \sqrt{M} \sum_{q=1}^{\infty} c_q x_{c+,q}$ , due to zero modes and plasmons, respectively. The lengthy but straightforward expressions of  $c_0$  and  $c_q$  will be deferred to a future publication [25]. We point out that Eq. (1) accounts for the coupling between vibron and density fluctuations  $H_{d-v}^{(pl)}$ , neglected in the AH model. The total Hamiltonian  $H_0 = H_d + H_v + H_{d-v}$  is thus quadratic in the generalized coordinates and is diagonalized [13, 26] (details will be given elsewhere [25]) into

$$\begin{aligned} H_0 &= \frac{E_c}{8}(N_{c+} - N_g)^2 + \frac{\pi v_F}{8L_d} [N_{c-}^2 + N_{s+}^2 + N_{s-}^2] + H_d^{(2)} \\ &+ \sum_{\nu \geq 0} \Omega_{\nu} a_{\nu}^{\dagger} a_{\nu} + \sum_{\mu \neq c+} \sum_{\nu \geq 1} \omega_{\mu,\nu} b_{\mu,\nu}^{\dagger} b_{\mu,\nu}. \end{aligned} \quad (2)$$

The sectors with  $\mu \neq c+$  are clearly unaffected by Eq. (1). On the contrary, in the  $c+$  sector new modes, created by  $a_{\nu}^{\dagger}$  with energies  $\Omega_{\nu}$  emerge. For  $\nu \geq 1$  they represent new collective electron modes (dressed plasmons), while for  $\nu = 0$  a vibronic excitation dressed by plasmons is obtained. The latter is the low-energy vibrational mode observed in the experiments. The energies  $\Omega_{\nu}$  satisfy  $\Omega_{\nu}^2 = \omega_0^2 + \sum_{q=1}^{\infty} c_q^2 / (\Omega_{\nu}^2 - \omega_{c+,q}^2)$ , with  $\Omega_0 < \omega_0$  and  $\Omega_{\nu} > \omega_{c+,\nu}$  for  $\nu \geq 1$  *always*. Note that we have reabsorbed a polaron shift into  $E_c$  [9].

*Local FC factors* — We can now study how the bosonized Fermi field  $\Psi_{R,\eta,\sigma}(y)$  [18] is affected by the transformation above. As we study tunneling at energies *smaller* than the collective charge and spin excitations of the dot, we restrict the Hilbert space to the  $\nu = 0$  mode of the sector  $c+$  only. Due to Eq. (1), the vibron operators  $a_{\nu}$  appear in the electronic field, whose truncated

form after the diagonalization reads [27]

$$\psi_{R,\eta,\sigma}(y) \approx \frac{\chi_{\eta,\sigma}}{\sqrt{2\pi\xi}} e^{-[\lambda_N + \lambda_-(y)][a_0^\dagger - a_0]} e^{i\lambda_+(y)[a_0^\dagger + a_0]}, \quad (3)$$

where  $\chi_{\eta,\sigma}$  decreases  $N_{\eta,\sigma}$  by one,  $\lambda_N = c_0/\sqrt{2M\Omega_0^3}$  and

$$\lambda_{\pm}(y) = \sqrt{\kappa \frac{\omega_{c+,1}}{\Omega_0} \sum_{q=1}^{\infty} \frac{c_q F_{\pm}(y)}{\Omega_0^2 - \omega_{c+,q}^2}} \quad (4)$$

with  $\kappa = 1 + \sum_{q=1}^{\infty} c_q^2 / (\Omega_0^2 - \omega_{c+,q}^2)^2$  and  $F_{\pm}(y) = \sin(\pi q y / L_d + \pi/4 \pm \pi/4)$ . Note that both  $\lambda_N$  and  $\lambda_{\pm}(y)$  depend on the CNT and dot parameters and position only via  $y_0$ , the length ratio  $\delta = L_v/L_d$ , the velocities ratio  $v_{c+}/v_s$ , and the dimensionless coupling  $\lambda_m = c/(v_s \sqrt{M\omega_0})$  [19]. The *local* FC factors [9, 13]  $X_{ll'}(y) = 2\pi\xi \langle N_{\eta,\sigma} - 1, l | \psi_{R,\eta,\sigma}(y) | N_{\eta,\sigma}, l' \rangle^2$  describing tunneling of an electron off the dot while changing the vibron number from  $l$  to  $l'$  ( $l \leq l'$ ) have the form

$$X_{ll'}(y) = e^{-\lambda^2(y)} [\lambda(y)]^{2(l'-l)} \frac{l!}{l'!} [L_l^{l'-l}(\lambda^2(y))]^2 \quad (5)$$

with  $\lambda^2(y) = [\lambda_N + \lambda_-(y)]^2 + \lambda_+^2(y)$  a *position-dependent* effective coupling and  $L_a^b(x)$  the generalized Laguerre polynomials. This is the main result of our paper. The position dependence is entirely due to the coupling between the vibron and the density fluctuations, neglected by the AH model which instead predicts *position-independent* FC factors, with constant interaction strength  $\lambda_N$ . When  $\max[\lambda_{\pm}(y)] \gg \lambda_N$  the position dependence cannot be neglected, and the AH model becomes questionable. This occurs for  $\delta = L_v/L_d < 1$  (which is the case of our experiment) and a vibron located *inside* the dot: in this case indeed  $\lambda_N = 0$ . Fig. 2a

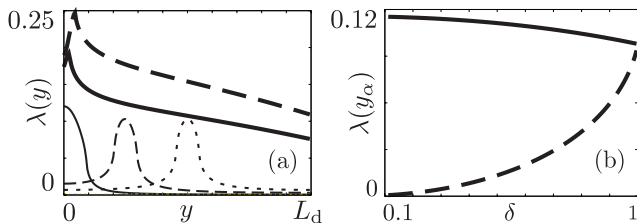


FIG. 2: (a) Plot of  $\lambda(y)$  for  $\delta = L_v/L_d = 0.1$  and different positions of the vibron center  $y_c = y_0 + L_v/2$ : (thick solid)  $y_c = -L_v/4$ ; (thick dashed)  $y_c = 0$ ; (thin solid)  $y_c = L_v/2$ ; (thin dashed)  $y_c = L_d/4$ ; (thin dotted)  $y_c = L_d/2$ . (b) Plot of  $\lambda(y_\alpha)$  vs.  $\delta$  ( $\alpha = 1, 2$ ) for  $y_0 = 0$  and  $\alpha = 1$  (solid);  $\alpha = 2$  (dashed). Notice the strong asymmetry for  $\delta \ll 1$  and the symmetric  $\lambda$ 's for  $\delta = 1$ . Here,  $v_{c+}/v_s = 32$  and  $\lambda_m = 3$  (for a CNT waist  $\simeq 1$  nm) [19].

shows  $\lambda(y)$  for  $\delta < 1$  and different locations of the vibron. When the latter sits inside the dot (thin lines, for  $0 < y_0 < L_d - L_v$ ),  $\lambda(y)$  is sizeable only in the vibron region. For vibrons partially outside the dot (thick lines),  $\lambda_N \neq 0$  and the position dependence of  $\lambda(y)$  is

weaker. For  $\delta > 1$  (not shown),  $\lambda_N \gg \lambda_{\pm}(y)$  which implies  $\lambda(y) \sim \lambda_N$ , and the *spatially-independent* FC factors of the AH model are obtained [15].

Of particular relevance for transport is the value of the coupling at the position of the tunneling barriers,  $\lambda(y_1)$  and  $\lambda(y_2)$ . For  $\delta < 1$  and a vibron located asymmetrically with respect to the dot center, they become very asymmetric (see the thin solid line of Fig. 2a), yielding strongly asymmetric FC factors. In Fig. 2b,  $\lambda(y_{1,2})$  are shown as a function of  $\delta \leq 1$  for a vibron located near the left barrier. The couplings are strongly barrier-dependent and vibrational excitations are strongly suppressed for tunneling on the right. In the symmetric case  $\delta = 1$ , dot and vibron occupy the same region of space and  $\lambda(y_1) = \lambda(y_2)$  [6]. Notice however that  $\lambda_N = 0$ .

The maximum value of the coupling for  $\delta < 1$  is crucially sensitive to the ratio  $v_s/v_{c+}$  and the value of  $\lambda_m$ . The coupling of the dot to the breathing mode reduces  $v_{c+}$  [6, 28], increasing  $v_s/v_{c+}$  and allowing to reach  $\lambda(y_1) > 1$  with  $\lambda(y_2) \ll 1$ . In parallel, recent measurements in graphene [29] report a large deformation potential, which further increases  $\lambda_m$ .

*Transport properties* — In order to address the electronic transport we introduce the tunneling Hamiltonian coupling the dot to the leads (represented by the CNT portions outside the dot)

$$H_t = \sum_{\alpha=1,2} \sum_{\eta,\sigma} t_{\alpha,\eta} \psi_{R,\eta,\sigma}^\dagger(y_\alpha) \Psi_{R,\eta,\sigma}(y_\alpha) + \text{h.c.},$$

where  $t_{\alpha,\eta}$  are tunneling amplitudes and  $\Psi_{R,\eta,\sigma}(y_\alpha)$  is the right movers field for lead  $\alpha$ . In sequential tunneling, transition rates are evaluated between eigenstates of  $H_0$  - Eq. (2). For tunneling *into* the state  $\eta$  of the dot through the barrier  $\alpha$  one has [14, 30]

$$\Gamma_{\alpha,\eta}^{(\text{in})} = \Gamma_0 \frac{|t_{\alpha,\eta}|^2}{|t_{2,+1}|^2} X_{ll'}(y_\alpha) f[\Delta E + (-1)^{\alpha+1} eV/2]$$

where  $\Gamma_0 = 2\pi\mathcal{D}|t_{2,+1}|^2/\xi^2$  and  $\mathcal{D}$  is the leads density of states, while  $f(E)$  is the Fermi function with  $\Delta E$  the energy difference between final and initial dot states. Similar expressions hold for tunnel-out processes.

The experiment allows to estimate the relevant parameters:  $E_c \approx 4.5$  meV (via Coulomb diamonds), the average  $\Gamma_0 \approx 1$   $\mu\text{eV}$  (via current traces),  $\Omega_0 \approx 800\mu\text{eV}$  (average vibron sideband separation) and  $k_B T \approx 90\mu\text{eV}$  (for  $T \approx 1$  K). Since  $k_B T \gg \Gamma_0$  the sequential regime is justified,  $\Omega_0 \gg k_B T$  allows to resolve vibronic excitations while  $\Omega_0 \gg \Gamma_0$  justifies a rate equation [14, 31] neglecting vibronic coherences [32]. The extremely rich scenario obtained for different asymmetries of left/right tunnel barriers  $A = |t_{1,\eta}|^2/|t_{2,\eta}|^2$  and of the coupling between leads and the two valleys  $\gamma = |t_{\alpha,-1}|^2/|t_{\alpha,+1}|^2$  will be discussed in detail elsewhere [25].

Here we focus on the relevant case to address the experimental data in Fig. 1. For  $V_g < 0$  in Fig. 1b, we found

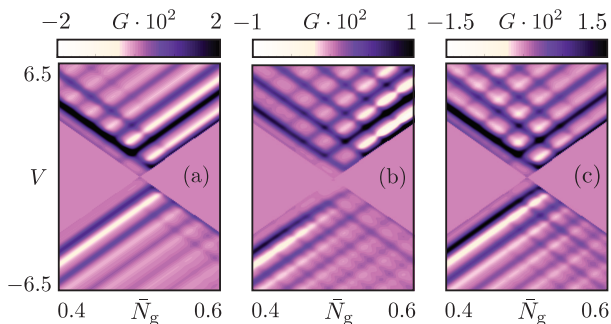


FIG. 3: (Color online) Plots of the numerical differential conductance  $G$  (units  $e^2/h$ ) as a function of  $\bar{N}_g = N_g - 3\pi v_F/2E_c L_d$  and  $V$  (units meV). (a) Density plot for  $A = 1/20$ ,  $\gamma = 20$ ,  $\lambda^2(y_1) = 2.4$ ,  $\lambda^2(y_2) = 0.1$ ; (b) same as in (a) but for  $\lambda^2(y_1) = \lambda^2(y_2) = 2.4$ ; (c) same as in (a) but for  $A = 1/5$ ,  $\lambda^2(y_1) = 1.8$  and  $\lambda^2(y_2) = 0.6$ . In all panels,  $\Omega_0 = 0.8$  meV,  $k_B T = 0.1 \Omega_0$ ,  $E_c = 4.5$  meV,  $\Delta\varepsilon = 0.48$  meV and  $\Gamma_0 = 0.8 \mu\text{eV}$ . For simplicity, only one resonance is shown.

that the *only possible parameter range compatible with experimental data* is:  $\lambda(y_2) \ll \lambda(y_1)$ ,  $A < 1$ ,  $\gamma > 1$  and  $\Delta\varepsilon > k_B T$ . The asymmetry of the FC factors is responsible for the strong suppression of negative-sloped sidebands, as clearly shown in Fig. 3a. We want to stress that the absence of traces with negative slope *is not* achievable in the standard AH model with *symmetric* FC factors, even in the presence of a quite strong asymmetry of the tunneling barriers, as shown in Fig. 3b. This proves the need to go beyond the AH model.

The alternating PDC/NDC traces can be addressed in our model by the three remaining constraints (on  $A$ ,  $\gamma$  and  $\Delta\varepsilon$ ). The NDC is due to the creation of a bottleneck in transport: when  $\gamma > 1$  tunneling into states  $\eta = +1$  is strongly suppressed leading to a dynamical trapping and NDC [33, 34], while the states  $\eta = -1$  provides a fast pathway with ensuing PDC. A shift of the two valleys  $\Delta\varepsilon > k_B T$  is necessary in order to resolve the two channels. Finally, the asymmetry  $A < 1$  allows to obtain the PDC/NDC pattern in all voltage regimes  $V \gtrsim 0$ .

Analyzing the experimental data, we observe that for  $V_g > 0$  the suppression of conductance traces becomes less severe (see Fig. 1c), suggesting more symmetrical FC factors as in Fig. 3c, in line with the standard AH model. In this case NDC traces with both positive and negative slopes occur for  $V > 0$ , pointing at an asymmetry  $A$  weaker than in Fig. 3a. The ultimate reason for the relative shift of electronic vs vibronic wavefunctions at different  $V_g$  lies in the unknown details of the electronic and mechanical confinements. Our predictions could stimulate further developments of experimental setups with full control over these delicate aspects.

*Conclusions* — Recent experimental data show the need of a theory *beyond* the usual Anderson-Holstein model of quantum transport in nano-electromechanical systems. Here we investigate this new issue by consider-

ing the combined role of the electronic charge and density fluctuations in the coupling to mechanical deformations for suspended CNT quantum dots. When vibrons are *asymmetrically* embedded into a *larger* dot, *position dependent* Franck-Condon factors arise. The consequent marked effects in the transport characteristics allow to address experimental features which could not be captured by the standard AH model. Our analysis can be easily extended to consider e.g. planar metallic contacts or the tunneling from a localized tip. For small vibrons embedded in larger dots a spatially-resolved injection of electrons would show a tunneling suppression sensitive to the vibron location, making our theory relevant for spatially-resolved scanning tunnelling microscope measurements as well. Similar effects could be expected also in systems of higher dimensionality, such as e.g. quantum dots embedded into suspended graphene sheets.

*Acknowledgments* — F. C. acknowledges support by INFN-CNR via Seed Project PLASE001. R. L. and C. S. thank K. Inderbitzin, L. Durrer, C. Hierold and K. Ensslin for help and support on the experiment.

- 
- [1] A. N. Cleland, Foundations of Nanomechanics (Springer, Berlin, 2003).
  - [2] B. J. LeRoy, S. G. Lemay, J. Kong, and C. Dekker, Nature **432**, 371 (2004).
  - [3] S. Sapmaz *et al.*, Phys. Rev. Lett. **96**, 026801 (2006).
  - [4] R. Leturcq *et al.*, Nature Phys. **5**, 327 (2009).
  - [5] A. K. Hüttel *et al.*, Phys. Rev. Lett. **102**, 225501 (2009).
  - [6] W. Izumida and M. Grifoni, New J. Phys. **7**, 244 (2005).
  - [7] K. Flensberg, New J. Phys. **8** 5 (2006).
  - [8] K. K. Viljas, J. C. Cuevas, F. Pauly, and M. Häfner, Phys. Rev. B **72**, 245415 (2005).
  - [9] A. Zazunov, D. Feinberg, and T. Martin, Phys. Rev. B **73**, 115405 (2006).
  - [10] X. Y. Shen, Bing Dong, X. L. Lei, and N. J. M. Horing, Phys. Rev. B **76**, 115308 (2007).
  - [11] J. Franck, Transactions of the Faraday Society **21**, 536 (1926); E. Condon, Phys. Rev. **28**, 1182 (1926).
  - [12] S. Braig and K. Flensberg, Phys. Rev. B **68**, 205324 (2003).
  - [13] A. Mitra, I. Aleiner, and A. J. Millis, Phys. Rev. B **69**, 245302 (2004).
  - [14] J. Koch and F. von Oppen, Phys. Rev. Lett **94**, 206804 (2005).
  - [15] E. Mariani and F. von Oppen, Phys. Rev. B **80**, 155411 (2009).
  - [16] R. Egger, Phys. Rev. Lett. **83**, 5547 (1999).
  - [17] M. Fabrizio and A. Gogolin, Phys. Rev. B **51**, 17827 (1995).
  - [18] H. Yoshioka and Y. Okamura, J. Phys. Soc. Japan **71**, 1812 (2002).
  - [19] Typical CNT parameters:  $c \approx 30$  eV,  $v_s \approx 2.4 \cdot 10^4$  m/s,  $v_F = 8 \cdot 10^5$  m/s and  $\rho_0 \approx 6.7 \cdot 10^{-7}$  Kg/m<sup>2</sup> [21]. Furthermore,  $v_{c-} = v_{s+} = v_{s-} = v_F$  and we assume  $v_{c+} \simeq v_F$  due to gate-induced screening.
  - [20] D. H. Cobden and J. Nygård, Phys. Rev. Lett. **89**, 046803

- (2002).
- [21] M. S. Dresselhaus and P. C. Eklund, *Adv. Phys.* **49**, 705 (2000).
- [22] H. Suzuura and T. Ando, *Phys. Rev. B* **65**, 235412 (2002).
- [23] The open boundary conditions allow a description in terms of right movers only [17, 18].
- [24] Note that Eq. (1) corresponds to Eq. (15) of Ref. 15.
- [25] F. Cavaliere *et al.*, in preparation.
- [26] P. Ullersma, *Physica* **32**, 27 (1966).
- [27] In these expressions we neglected phase factors, irrelevant for our analysis.
- [28] A. De Martino and R. Egger, *Phys. Rev. B* **67**, 235418 (2003).
- [29] K. Bolotin *et al.*, *Phys. Rev. Lett.* **101**, 096802 (2008).
- [30] F. Haupt, F. Cavaliere, R. Fazio, and M. Sassetti, *Phys. Rev. B* **74**, 205328 (2006).
- [31] M. Merlo, F. Haupt, F. Cavaliere, and M. Sassetti, *New J. Phys.* **10**, 023008 (2008).
- [32] For NDC in the coherent regime see e.g. G. Begemann *et al.*, *Phys. Rev. B* **77**, 201406(R) (2008); M. G. Schultz and F. von Oppen, *Phys. Rev. B* **80**, 033302 (2009).
- [33] M. Ciorga *et al.*, *Appl. Phys. Lett.* **80**, 2177 (2002).
- [34] F. Cavaliere *et al.*, *Phys. Rev. Lett.* **93**, 036803 (2004).